THE ATLANTIC-WIDE RESEARCH PROGRAMME FOR BFT (GBYP Phase 13)

SHORT-TERM CONTRACT (ICCAT GBYP 05/2023)

Design- based inference to estimate density, abundance, and biomass of bluefin tuna in the Mediterranean Sea. Analysis including the 2023 aerial visual surveys.

Final Report

April 2024

CREEM, University of St Andrews

M. Chudzińska, C. G. M. Paxton, L. Burt

Please cite this report as: Chudzińska *et al*. (2024). Design- based inference to estimate density, abundance, and biomass of bluefin tuna in the Mediterranean Sea. Analysis including the 2023 aerial visual surveys. Report number CREEM-2024-03. Provided to ICCAT, April 2024 (Unpublished).

Document control

Please consider this document as uncontrolled copy when printed.

Version	Date	Reason for issue	Prepared by	Checked by
1	3 April 2024	First draft	LB, CP, MC	LB, CP

CREEM
Centre for Research into Ecological and Environmental Modelling

University of St Andrews

Co-funded by the European Union

1 Contents

2 Introduction

This report presents analysis of the visual aerial survey data collected to obtain estimates of Bluefin tuna (BFT) in the Mediterranean Sea in the three surveyed blocks (A, C and E) in 2023, and updates the estimates from the previous surveys conducted in 2017-2022. Abundance and biomass in the surveyed blocks were estimated using line transect distance sampling methods (sensu Buckland et al. (2001)).

The tuna indices are updated in two ways: actualisation (Task 1), and strict update (Task 2). These are described below.

2.1.1 Task 1: Actualisation of the tuna indices.

Paxton et al. (2023) estimated density, biomass and abundance (referred to as 'indices') of BFT for the Mediterranean Sea survey blocks for years 2017-2022 and compared them to the estimates from the previous analysis (Chudzinska et al. 2021, Chudzinska et al. 2022). Although aerial surveys in region G (southern coast of Turkey) of the Mediterranean Sea stopped being conducted in 2019, including these data in the actualisation of the indices results in different estimates compared to excluding these data from the analysis (Paxton et al. 2023).

In Task 1 we added the aerial survey data collected on 2023 (in blocks A, C and E) to data collected in years 2017-2022. Line transect distance sampling methods (Buckland et al. 2001) were used to estimate density, abundance and biomass for blocks A, C and E for the years 2017- 2023. In addition, we added data from block G (collected in years 2017-2019) and obtained estimates for 2017-2023 for all blocks.

2.1.2 Task 2: Strict update of the tuna indices.

Building a detection function based on an updated data set (here, an additional year of data collected in 2023), may result in different covariates (explanatory variables) being retained in the final model compared to a model estimated without the additional data. Alternatively, it may result in the same covariates being retained in the final model but the values of the coefficients for these covariates will differ compared to the model with the same covariates but based on reduced data set. Consequently, a detection function based on the updated data set may result in different estimates of tuna indices compared to indices for previous years obtained without the additional data.

To provide a strict update, the detection function from last year (Paxton et al. (2022)) (i.e. the same variables and same parameters) were used to obtain alternative estimates for 2023 abundance and biomass respectively.

3 Methods

3.1 Overview of the aerial surveys

Three blocks, A, C and E (Figure 1), were surveyed in 2023. Details on survey protocols and outcomes are provided by AirPerigord (2023), Unimar and AerialBanners (2023b, 2023a), here we provide only information relevant for this report. Table 1 summarises the timing, number, and total length of search effort, company and airplane type used for BFT surveys in 2023. The survey in 2023 was conducted by the same companies and using the same type of aircrafts as 2022 survey (Paxton et al. 2023). Note that due to unfavourable weather conditions, block E was only partially surveyed (Figure 4).

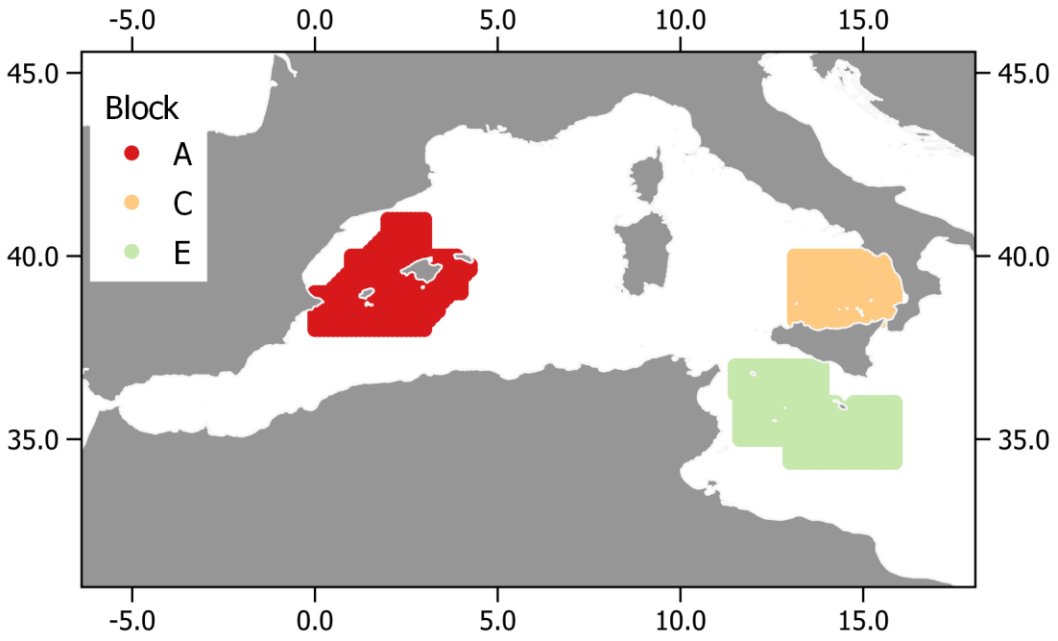

Figure 1. Depiction of Mediterranean Sea and the three survey blocks.

Table 1. Summary of the blocks and survey design in 2023 survey.

Year	Block	Dates	Number of transects	Search effort [km]	Company	Airplane
2023	A	01 June – 26 June	29	5277.0	Air Perigord	Cessna
	C	02 June – 19 June	25	5015.4	Unimar/Aerial Banners	Partenavia
	E	20 June – 05 July	21	5181.3	Unimar/Aerial Banners	Partenavia

3.2 Statistical methods - Distance sampling (DS)

3.2.1 Survey design

As for previous surveys, we obtained perpendicular distances to the line for the 2023 sightings using the trigonometric relationship:

$$y_i = h_i * \tan((90 - \theta_i)$$

where y_i i is the perpendicular distance between the transect and the i th school, θ_i i is the declination angle measured when the plane was a beam and h_i is the height of the airplane above sea level when abeam (Figure 2).

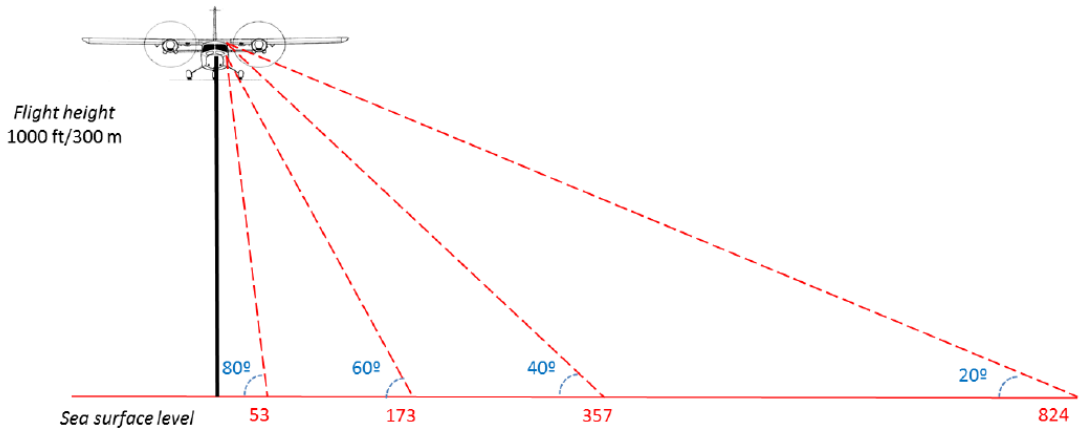

Figure 2. Example of the key declination angles and perpendicular distances at an altitude of h = 1000 ft = 300 m (Figure 5 from ICCAT survey protocol. Source: https://www.iccat.int/.)

For consistency with the analysis of the data from the previous years, all sightings from 2023 were truncated to 1500 m. The final distribution and number of the detections from 2023 and 2017-2023 after truncation is given in Figure 3 and Table 3.

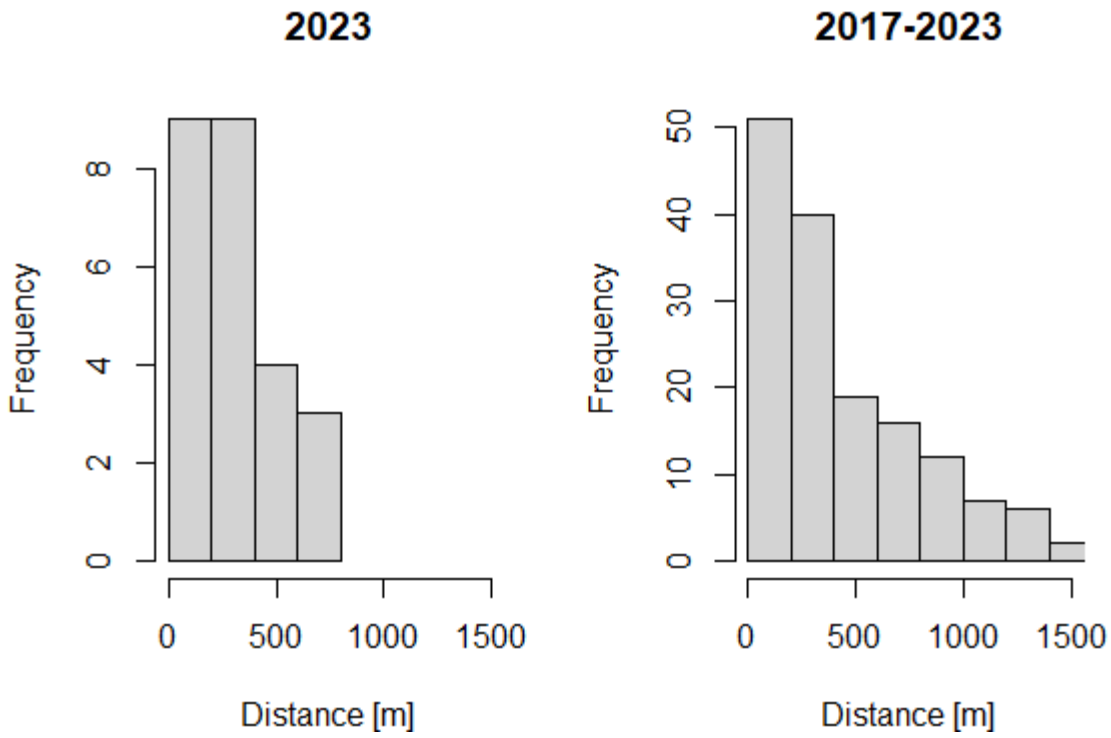

Figure 3. Distribution of perpendicular distances within 1500 m from the transect for 2023 only (left) and combined 2017-2023 (right).

3.2.2 Fitting the detection function

Two critical assumptions of DS methods are that all schools on the transect (i.e., at zero perpendicular distance) are detected with certainty and that distance measurements are exact (i.e., measured without error). Given these assumptions, the distribution of perpendicular distances is used to model how the probability of detection decreases with increasing distance from the transect. The former assumption can be relaxed to allow estimation of relative numbers of animals.

Perpendicular distances were right truncated to 1500 m, to avoid a long tail in the detection function. The choice of this truncation distance was based on visual inspection of fitted detection function and comparison with truncation distance used for previous years (2017-2022 models, Paxton et al. (2023)). No left truncation was applied; left truncation is a common practice for aerial surveys, due to difficulties in searching directly underneath the plane, especially when the plane does not have a bubble window, which was not the case with the aerial surveys under consideration.

The analysis was performed in R version 4.2.1 (R Core Team 2023) using the packages Distance (Miller 2022) and mrds (Laake et al. 2020).

3.2.2.1 Task 1

Two detection functions were fitted: A. to sightings from 2017-2023 from blocks A, C, E and G, and B. to sightings from 2017-2023 from blocks A, C, and E. We tested the fit of two key functions, the half normal (hn) and the hazard-rate (hr) and investigated whether adding covariates to the model in a multiple-covariate distance sampling (MCDS; e.g. Marques et al. 2007) approach would improve model fit. Here, five covariates which may affect the observers' ability to detect school were considered: the log of school size (*log-size*), the company conducting the survey (*company*), the type pf plane used (*airplane*), year in which the survey took place (*year*), and a combination of survey block (A, C or E) with survey year (*block*) (Table 2). We used log of the school sizes due to large variation in observed sizes ranging from 1 to 4000 individuals (Figure 5). Because environmental data (e.g. sea state) were not provided for the sightings, they were not included as covariates. Model selection was based on minimum AIC values, but if a simpler model was within 2 AIC units of the minimum model, then the simpler model was selected (Akaike 1987).

Table 2. Covariates considered for multiple-covariate distance sampling analyses.

Covariate	Description
log-size	Log of school size
company	Factor with five levels (Airmed, Unimar, ActionAir, Air Perigord, Unimar/Aerial Banners)
airplane	Factor with two levels (Partenavia, Cessna)
year	Factor with six levels (2017, 2018, 2019, 2021, 2022, 2023)
block-year	Block-year combination (factor)

Initially, models without any covariates (null models) were fitted. We then fitted single covariate models to both key functions using the five available covariates. Finally, we fitted models which included a combination of log-size and each of the remaining covariates. This process was consistent with model fitting conducted in the previous years (Paxton et al. 2023).

To assess goodness of fit of the model, various options can be explored with the Distance package (Miller 2022): a quantile-quantile (Q-Q) plot and various tests, including χ^2, Kolmogorov-Smirnov and Cramer-von Mises tests (in function gof_ds), whereby large *p*-values indicate a good fit to the observed data (Miller et al. 2019, Laake et al. 2022).

Sightings and search effort were pooled within each block to obtain encounter rates, and hence obtain estimates of density and abundance, by year (for 2017-2023 combined models). Estimates averaged overall surveys (weighted by survey effort) were also obtained.

The same approach was used to estimate biomass. In this case the size of observed schools was replaced by the estimated biomass. As in the analysis in the previous years, only sightings from professional observers were used.

The lengths of the realised transects were calculated from the recorded positions (i.e. latitude and longitude), when observers were on search effort. Only schools sighted when observers were on search effort and within 1500 m were included in the analysis.

Although only part of the block E was surveyed in 2023, the predictions of the abundance and biomass were made for the area surveyed in the previous years (2017-2022). This assumes that the unsurveyed portion of block E was like the portion surveyed in terms of number of detected schools and their abundance and biomass.

3.2.2.2 Task 2

In the previous report (Paxton et al. 2023), the variables selected in the detection function were *company* and *log-size* to estimate tuna abundance and *company* and *log-biomass* for to estimate tuna biomass. These detections functions (i.e., using the same model parameter values) were applied to obtain estimates for 2023. Note that last year's strict update estimates used both data from blocks A, C, E and G, as well as A, C, and E only. In Task 2 we used detection function estimated for all four blocks.

4 Results

4.1 Summary of search effort, encounter rate and sightings for 2023 data

Table 3 summarises the sightings for the 2023 survey. Like previous years, most sightings in 2023 were observed in block A. For the distance sampling analysis, we only use on-effort sightings and sightings of non-juveniles' schools. Sightings described as 100% small (individuals <25 kg) have, therefore, been excluded, however, the remaining sightings may still include some schools that contain small individuals amongst larger fish. The final number of sightings is presented in Table 3 and their location as well as transect location are depicted in Figure 4.

Table 3. Summaries of BFT sightings in 2023. The *Final number* indicates the number of sightings which are on-effort and represent adult schools. In brackets are given numbers after truncation to 1,500 m.

Year	Block	All sightings	On effort	Non juveniles	Final number
2023	A	24	22	22	21 (14)
	C	5	5	4	4 (3)
	E	11	11	8	8 (8)

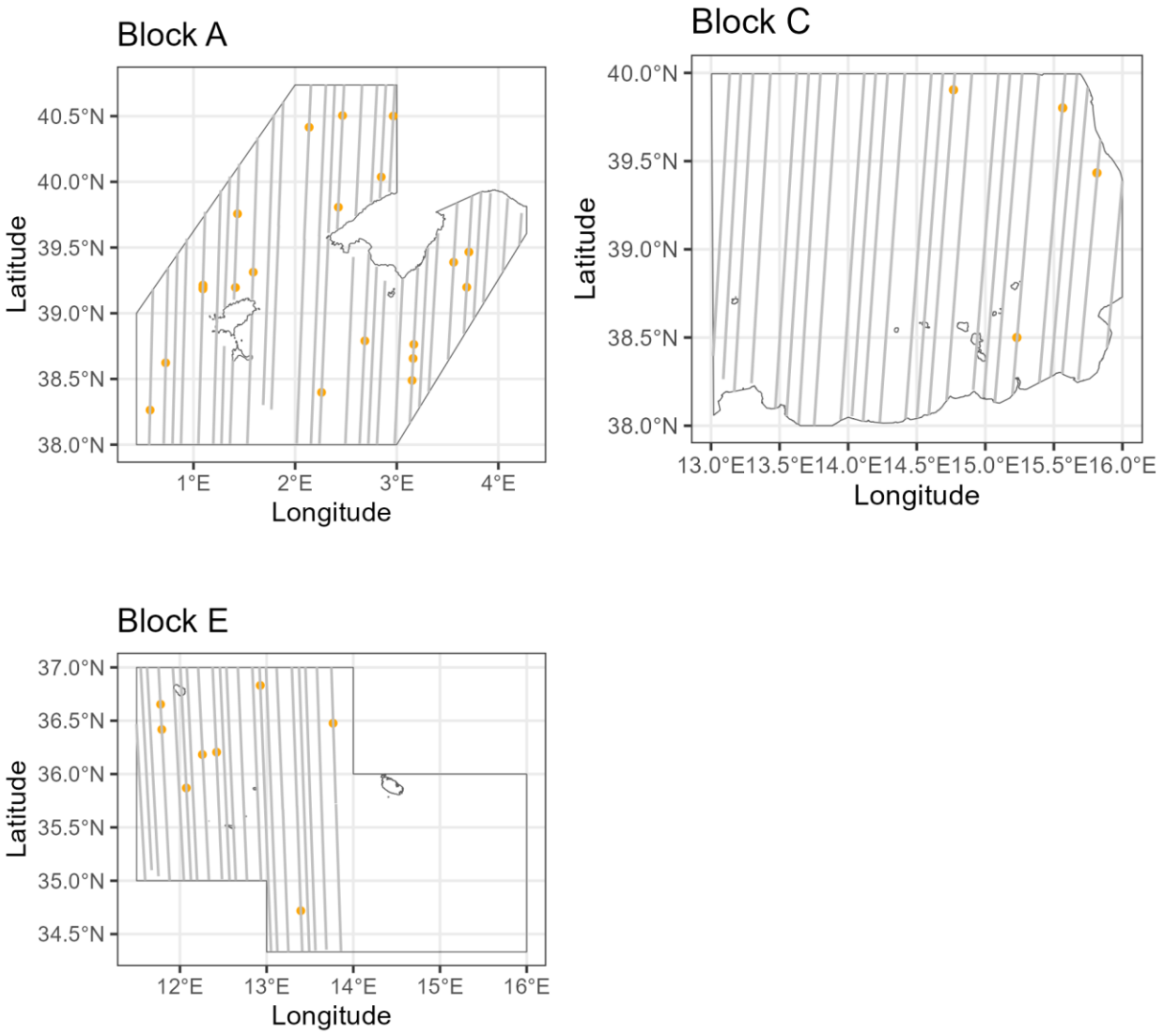

Figure 4. 2023 survey transects (grey lines) and sightings (orange dots) used for the final design-based analysis for the three blocks: A, C and E. The sightings represent on-effort sightings of adult schools before truncation. Due to unfavourable weather conditions, block E was surveyed only partially.

The school sizes observed in 2023 were, on average, larger than in the previous years. This was also reflected in the larger average observed biomass, second only to year 2021 (Figure 5).

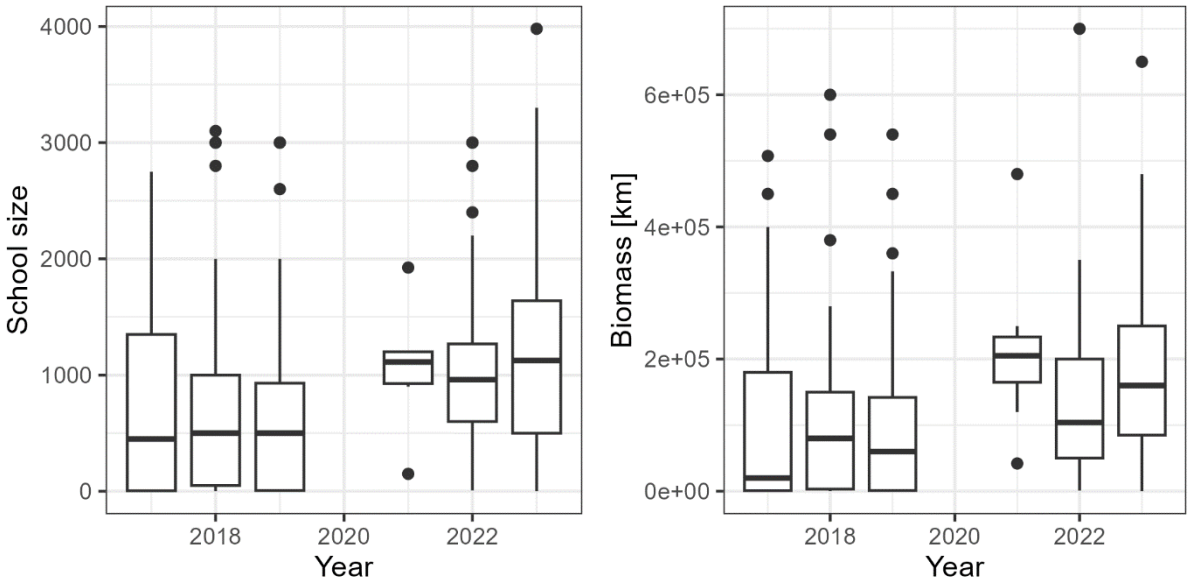

Figure 5. Distribution of observed school sizes (left) and their biomass (right) in 2017-2023 surveys. Only sightings marked as 'Final number' (before truncation) in Table 3 are shown. Outliers are more than 1.5. times the interquartile range from the central box.

The largest search effort per block was conducted in block A and lowest in block C (Table 4). Apart from block E, which was only surveyed partially (Figure 4), the effort and area covered in each block was comparable to these in the previous years (Table 7 in Paxton et al. 2023). Most sightings were made in block A, resulting in the highest estimated encounter rates and with lowest CVs. Encounter rate estimates were lowest in block C with highest CVs.

Table 4. Summary per block of area covered by the survey, effort conducted, number of schools encountered within 1500 m (n), number of transects (k), estimated encounter rate (ER) and its standard deviation (SE) and CV (CV).

Block	Area (km^2)	Covered Area (km^2)	Effort (km)	n	k	ER	SE	CV
A-2023	61837	15831.2	5271	14	29	0.0027	0.00087	0.32
C-2023	53868	15046.0	5015.0	3	25	0.0006	0.00033	0.56
E-2023	93614	15543.6	5181.5	8	21	0.0015	0.00052	0.34

Estimated numbers of schools (N_G) per block were highest again in block A but the lowest CVs were for block E (Table 5). Estimated number of schools was lowest in block C and this estimate for this block was much lower than the estimate from the previous survey in 2022 (Table 8 in Paxton et al. 2023). The number of schools for block E is, on the other hand, higher than estimate from the survey in 2022.

The expected school sizes were lowest in block A and highest in block E (Table 5). The estimate was lower for blocks A and C and higher for block E than the estimate from the previous survey in 2022 (Table 8 in Paxton et al. 2023).

Table 5. Average probability of detection (p), number of schools encountered (n), estimated number of schools N_G per block along with its standard error (SE), coefficient of variation (CV), lower and upper 95% confidence limits (LCL and UCL), expected school size (E_{size}) and its standard error (SE_E)).

Block	p	n	N_G	SE	CV	LCL	UCL	E_{size}	SE_E
A-2023	0.32	14	166.4	67.5	0.40	75.9	364.5	358.9	160.9
C-2023	0.35	3	30.0	17.9	0.59	9.7	92.6	1104.9	479.8
E-2023	0.37	8	128.1	48.3	0.37	61.0	269.1	1166.1	167.5

4.1.1 Task 1A – analysis based on all blocks (A, C, E and G)

4.1.1.1 Detection function for abundance and biomass

The detection function models tested are shown in Table 6. Models including *log-size* and one of the other covariates had lower AIC than models including one covariate at the time for abundance. Such a pattern was not present for biomass. From the models which had two covariates, the hazard-rate one including *log-size* and *block-year* had lowest AIC both for abundance and biomass. As the difference in AIC units (Δ AIC) between this model and the half-normal one including *log-size* and *company* is less than 2, for the consistency with detection function from the previous reports (Chudzinska et al. 2021, Chudzinska et al. 2022, Paxton et al. 2023), we take the latter model as the final one both for abundance and biomass (Table 6).

Table 6. Models tested for school size for 2017-2023 sightings including blocks A, C, E and G. Δ AIC refers to the difference between a given model and the model with lowest AIC. The final selected model is marked in bold. 'Key' refers to two key functions: hazard rate (hr) and half-normal (hn). The models are sorted by Δ AIC of the abundance detection function.

Models	Key	Δ AIC (abundance)	Δ AIC (biomass)
log-size + block-year	hr	0	0
log-size + company	**hn**	**1.7**	**1.6**
log-size + block-year	hn	7.5	5.1
log-size + company	hr	11.4	8.3
log-size + plane	hn	12.7	10.2
log-size + year	hn	16.7	
log-size	hn	17.6	23.3
log-size + plane	hr	23.7	146.4
log-size + year	hr	25.1	154.4
log-size	hr	28.4	144.4
block-year	hr	38	27.1
company	hr	43.4	32.5
plane	hr	54.5	43.6

block-year	hn	54.6	43.7
Null	hn	55.1	44.2
Null	hr	56.4	45.1
year	hr	63.2	52.3
year	hn	65.6	54.2
plane	hn	67.7	56.8
company	hn	67.9	57.2

The histogram of perpendicular distances showed a relatively steep decline in detection probabilities between 0 and 500 m (Figure 6). This was mostly driven by the sightings with small school sizes, shown in the figure as those below the histogram line, i.e. lower than average detection probabilities. Most of these small school sizes were detected in Block A by company Airmed. This company surveyed block E in 2017 and block A in 2018-2019. A similar pattern applies to biomass. The schools observed by Airmed that were close to the transect has lower biomass than observed by other companies.

The fit of the best detection function model (Table 6) to the observed data was deemed adequate as judged by the Q-Q plot (Figure 7Figure 6) and the three goodness of fit test statistics including the χ^2 test (using 20 equally-spaced distance bins), the Kolmogorov-Smirnov test (with 100 bootstrap samples) and the Cramer-von Mises test (Table 7) for both abundance and biomass.

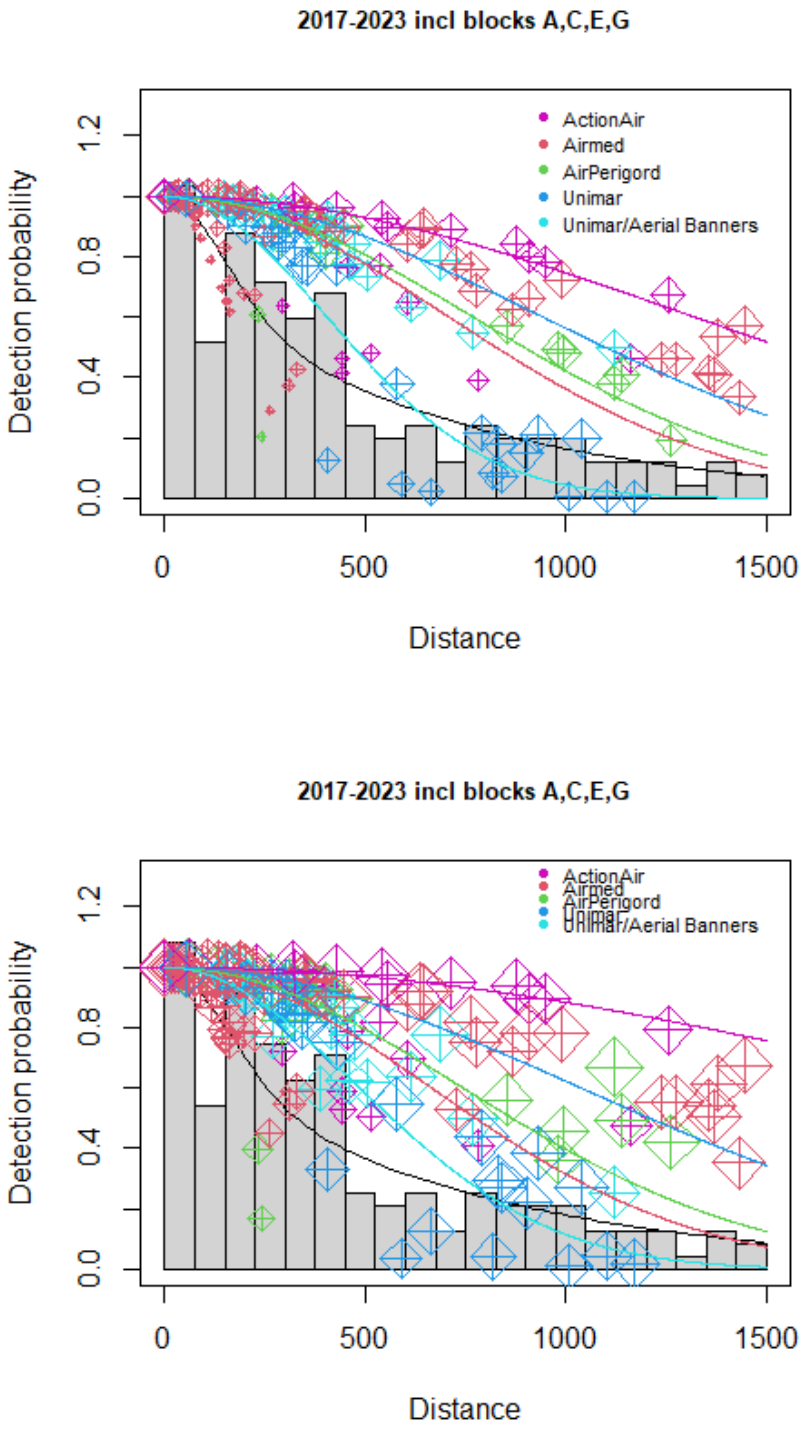

Figure 6. Histogram of observed distances, average detection function across all observations (histogram black line) and detection probabilities of observed distances from best fitting model colour coded by company. Size of symbols were scaled to represent the natural log of school size (top panel) and log biomass (bottom panel) detected by each company.

Table 7. Goodness of fit tests and results conducted to assess fit of best detection function model.

Test	Test statistic abundance	p-value abundance	Test statistic biomass	p-value biomass
χ^2 (13 degrees of freedom)	14.1	0.23	16.8	0.21
Kolmogorov-Smirnov	0.04	0.73	0.05	0.7
Cramer-von Mises	0.05	0.85	0.09	0.63

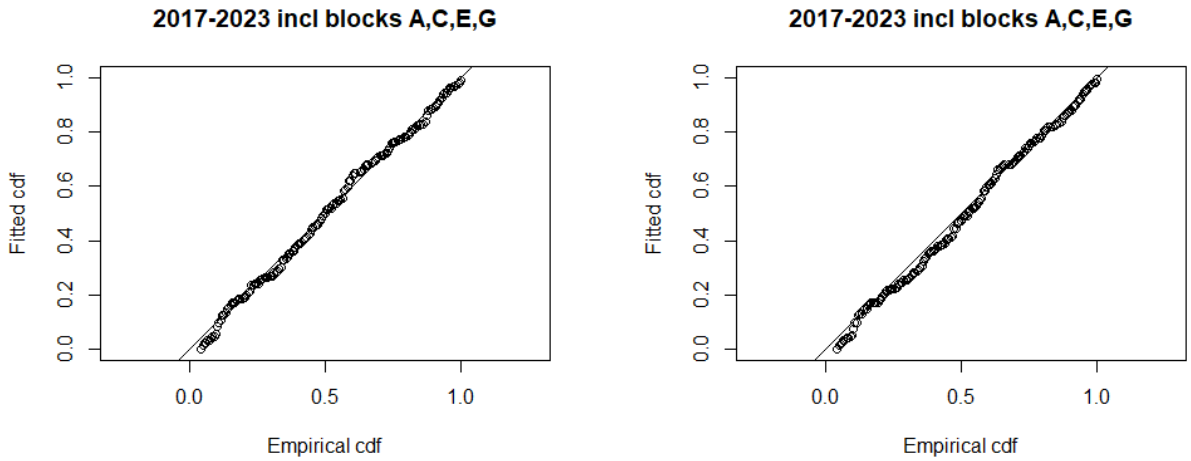

Figure 7. Q-Q plot for best fitting model showing the observed (empirical) cumulative distribution function (ECDF) against the fitted CDF (FCDF) along with a line of best fit (y=x line) for abundance (left) and biomass (right).

4.1.1.2 Estimated abundance for years 2017-2023.

For blocks A and E, there is an increase in estimated abundance in comparison with estimates from 2022 and a sharp decrease for block C. Block C also showed the largest change in abundance in comparison to previous years. The estimates for this block for 2023 are associated with larger CVs that the estimates for the other two blocks in that year (Table 8, Figure 8). Figure 8 shows comparison between current estimates and estimates of the abundance from the previous two reports. The current results are comparable with the previous estimates.

Table 8. Estimated number of individual tuna (N, in thousands) per block (block and year) with standard errors (SE) and lower (LCL) and upper (UCL) confidence levels. Coefficient of variation (CV) is also provided for the results from this analysis. The orange values apply to estimates reported in Paxton et al. 2023, and the grey values in Chudzinska et al. 2022. All estimates are based on sightings from all blocks: A, C, E and G.

Label	N	SE	CV	LCI	UCI	N	CV	LCI	UCI	N	CV	LCI	UCI
	This report					Paxton et al. 2023				Chudzinska et al. 2022			

A-2017	51.6	22.0	0.4	22.8	117.0	48.9	0.43	21.5	111.3	49.9	0.4	21.8	114.2
A-2018	84.4	25.3	0.3	47.0	151.5	79.9	0.3	44.2	144.6	81.6	0.3	45.3	147.1
A-2019	79.8	31.4	0.4	37.3	170.7	75.7	0.4	35.3	162.7	75.0	0.4	36.7	153.3
A-2021	29.3	15.8	0.5	10.6	80.8	26.3	0.53	9.8	71.1	26.1	0.5	9.6	71.1
A-2022	39.4	15.1	0.4	18.8	82.5	35.1	0.38	15.1	81.5				
A-2023	59.7	28.0	0.5	24.1	147.6								
C-2017	45.4	18.6	0.4	20.4	101.1	44.1	0.41	19.9	97.9	44.9	0.4	19.5	103.2
C-2018	37.7	21.6	0.6	12.7	112.4	36.8	0.57	12.4	109.2	37.4	0.5	13.7	101.8
C-2019	26.3	15.2	0.6	8.7	79.4	25.5	0.58	8.5	77.0	26.0	0.6	8.4	80.0
C-2022	158.4	64.9	0.4	71.2	352.5	167.8	0.42	74.2	379.4				
C-2023	33.2	22.3	0.7	9.5	115.8								
E-2017	45.5	23.5	0.5	17.1	121.1	42.1	0.52	15.8	112.7	44.1	0.5	16.4	118.7
E-2018	40.4	23.7	0.6	13.6	120.2	39.2	0.59	13.2	116.6	40.1	0.5	16.6	96.71
E-2019	19.0	9.0	0.5	7.7	46.8	31.2	0.5	12.1	80.2	17.9	0.5	7.0	45.7
E-2022	45.3	35.3	0.8	11.2	183.3	22.9	0.83	5.2	99.8				
E-2023	149.4	61.0	0.4	67.0	333.2								

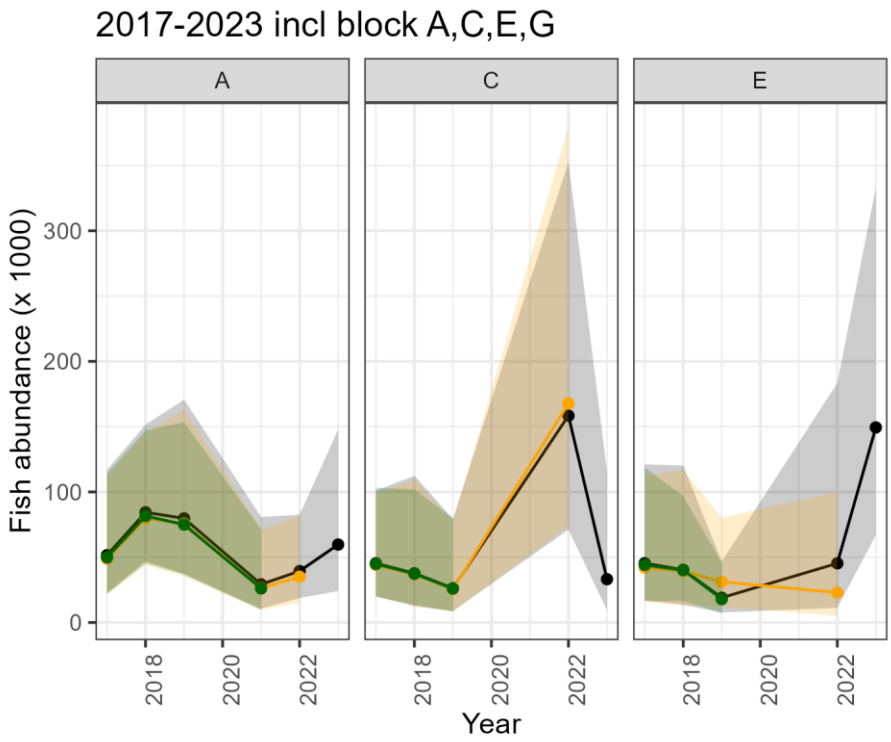

Figure 8. Estimated abundance of BFT for surveyed years and blocks. Black colours show estimates from this study: dots show mean values and ribbon show upper and lower confidence limits of the 95% confidence interval. Orange colour shows estimates from the previous report (Paxton et al. 2023) and green the second last report (Chudzinska et al. 2022).

4.1.1.3 Estimated biomass for years 2017-2023.

The biomass estimates are presented in Table 9 and Figure 9. The estimates for the previous years based on the newest detection function are comparable with the estimates from the previous reports. There is no increase in biomass in block A in 2023 despite the increase in abundance from 2022. There is a sharp decrease in biomass in block E and a sharp increase in block C following these trends in abundance (Figure 8, Figure 9).

Table 9. Estimated biomass (B, in tonnes) per block (block and year) with standard errors (SE) and lower (LCL) and upper (UCL) confidence levels. Coefficient of variation (CV) is also provided for the results from this analysis. The orange values apply to estimates reported in Paxton et al. 2023, and the grey values in Chudzinska et al. 2022. All estimates are based on sightings from all blocks: A, C, E and G.

Label	B	SE	CV	LCI	UCI	N	CV	LCI	UCI	N	CV	LCI	UCI
	This report					Paxton et al. 2023				Chudzinska et al. 2022			
A-2017	8726	3817	0.44	3774	20177	7949	0.44	3426	18444	8001	0.45	3436	18634
A-2018	14603	4480	0.31	8034	26544	13251	0.31	7225	24304	13345	0.31	7352	24222
A-2019	12948	5139	0.40	6015	27871	11808	0.40	5469	25495	11548	0.38	5619	23734
A-2021	5183	2747	0.53	1905	14105	4955	0.53	1831	13410	4714	0.53	1750	12696
A-2022	10640	4849	0.46	4441	25493	9433	0.49	3723	23899				
A-2023	10970	5364	0.49	4289	28056								
C-2017	6994	2824	0.40	3167	15442	6715	0.40	3060	14733	6749	0.43	2981	15280
C-2018	5238	3032	0.58	1740	15767	5042	0.58	1680	15129	5069	0.54	1846	13920
C-2019	3186	1857	0.58	1047	9696	3057	0.58	1008	9275	3072	0.62	977	9652
C-2022	10770	4610	0.43	4677	24804	9965	0.44	4237	23436				
C-2023	4054	2764	0.68	1140	14412								
E-2017	6393	3726	0.58	2147	19040	5822	0.58	1951	17372	5884	0.6	1981	17483
E-2018	3865	2205	0.57	1335	11189	3702	0.57	1283	10682	3735	0.47	1538	9067
E-2019	2096	994	0.47	848	5176	1956	0.46	804	4760	2023	0.5	797	5188
E-2022	2110	1599	0.76	537	8284	2092	0.77	528	8293				
E-2023	14954	6592	0.44	6299	35500								

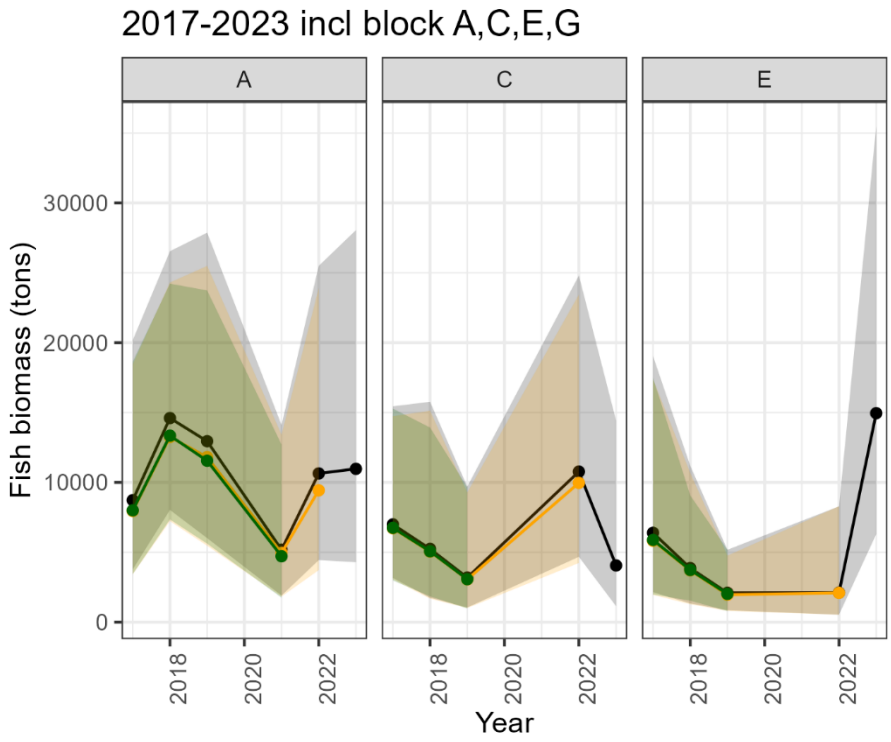

Figure 9. Estimated biomass (in tonnes) of BFT for surveyed years and blocks. Black colours show estimates from this study: dots show mean values and ribbon show upper and lower confidence limits of the 95% confidence interval. Orange colour shows estimates from the previous report (Paxton et al. 2023) and green the second last report (Chudzinska et al. 2022).

4.1.2 Task 1B – analysis based on three blocks (A, C, and E)

4.1.2.1 Detection function for abundance and biomass

Models tested are shown in Table 10 and these are the same model formulations as for the analysis based on all four blocks. Models including *log-size* and one of the other covariates had lower AIC that models including one covariate at the time for abundance and biomass. From the models which had two covariates, the hazard-rate one including *log-size* and *block-year* had lowest AIC both for abundance and biomass. As the delta AIC between these models and half-normal one including *log-size* and *company* is < 2, for the consistency with detection function from the previous reports (Chudzinska et al. 2021, Chudzinska et al. 2022, Paxton et al. 2023), we take the latter model as the final one both for abundance and biomass (Table 10).

Table 10. Models tested for school size for 2017-2023 sightings including blocks A, C and E. Δ AIC refers to the difference between a given model and best (bold). Key refers two key functions: hazard rate (hr) and half-normal (hn). The models are sorted by Δ AIC of the abundance detection function.

Models	Key	Δ AIC (abundance)	Δ AIC (biomass)

log-size + block-year	hr	0.0	0
log-size + company	**hn**	**1.5**	**1.4**
log-size	hn	9.1	3.3
log-size + plane	hn	11.0	5.2
log-size + block-year	hn	1.3	3.4
log-size + year	hn	12.4	7.9
log-size + company	hr	12.9	12.8
log-size	hr	19.2	13.8
log-size + year	hr	20.6	16.6
log-size + plane	hr	21.0	15.8
block-year	hr	35.1	24.9
company	hr	44.8	34.6
block-year	hn	51.6	41.5
null	hn	52.6	42.5
null	hr	54.0	43.8
plane	hr	55.0	44.8
year	hr	57.9	56.7
year	hn	66.8	59.6
plane	hn	69.7	59.6
company	hn	70.0	59.8

As for detection function based on all four blocks, the histogram of detections showed a relatively quick drop off in detection probabilities between 0 and 500 m (Figure 10). This was mostly driven by the detections with small school sizes, shown in the figure as those below the histogram line, i.e. lower than average detection probabilities. Most of these small school sizes were detected in Block A by company Airmed. This company surveyed block E in 2017 and block A in 2018-2019. A similar pattern applies to biomass. The schools observed by Airmed close to the tracks has lower biomass than observed by other companies.

The fit of the best detection function model (Table 11) to the observed data was deemed adequate as judged by the Q-Q plot (Figure 11Figure 6) and the three goodness of fit test statistics including the χ^2 test (using 20 equally-spaced distance bins), the Kolmogorov-Smirnov test (with 100 bootstrap samples) and the Cramer-von Mises test (Table 11) for both abundance and biomass.

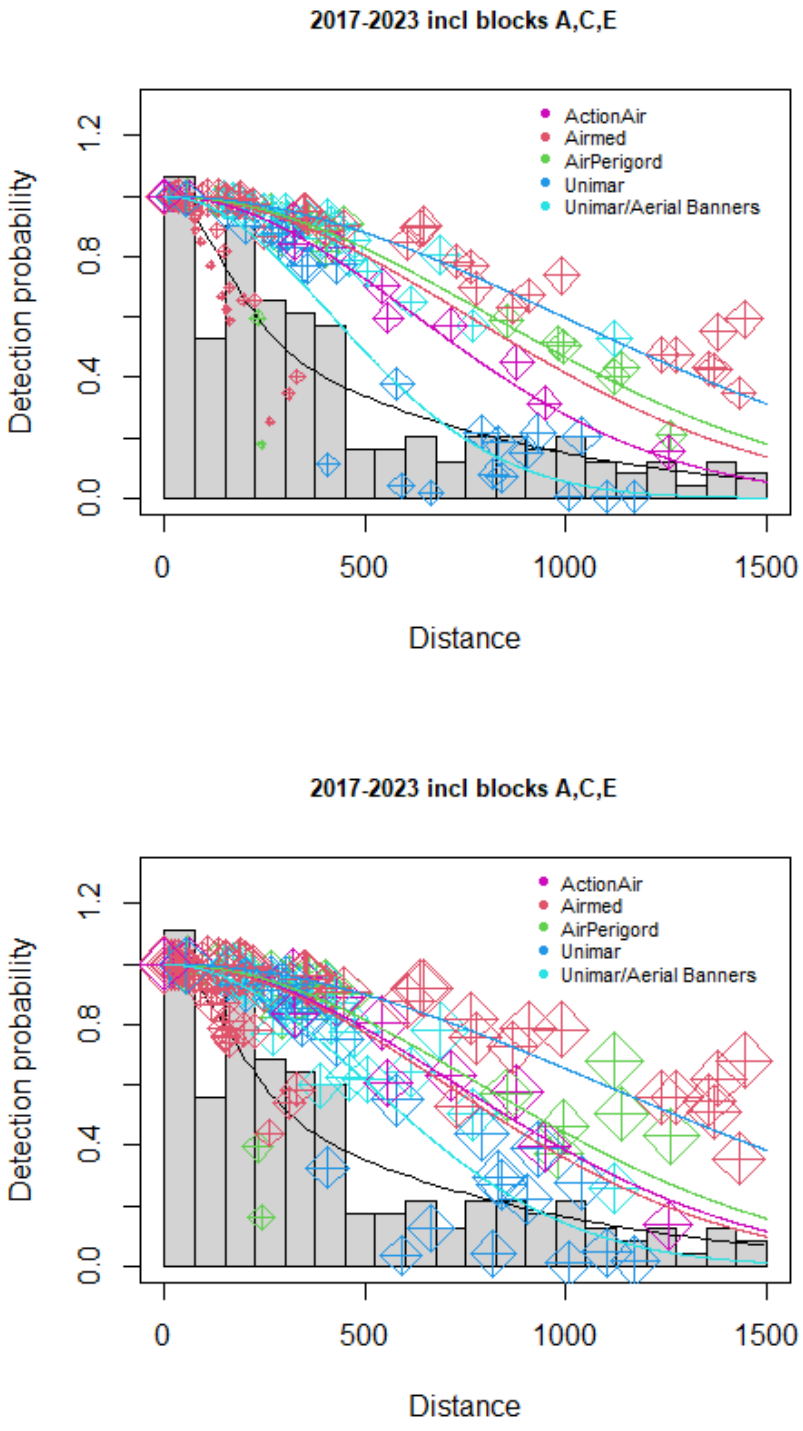

Figure 10. Histogram of observed distances, average detection function across all observations (histogram black line) and detection probabilities of observed distances from best fitting model colour coded by company. Size of symbols were scaled to represent the natural log of school size (top panel) and log biomass (bottom panel) detected by each company.

Table 11. Goodness of fit tests and results conducted to assess fit of best detection function model.

Test	Test statistic abundance	p-value abundance	Test statistic biomass
X^2 (13 degrees of freedom)	16.9	0.20	16.6
Kolmogorov-Smirnov	0.05	0.86	0.07
Cramer-von Mises	0.07	0.75	0.13

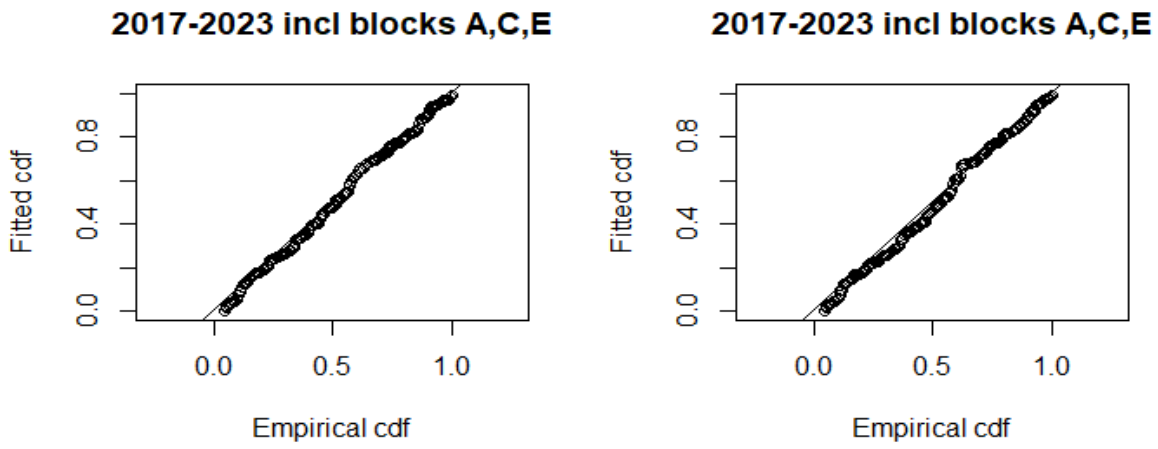

Figure 11. Q-Q plot for best fitting model showing the observed (empirical) cumulative distribution function (ECDF) against the fitted CDF (FCDF) along with a line of best fit (y=x line) for abundance (left) and biomass (right).

4.1.2.2 Estimated abundance for years 2017-2023.

For blocks A and E, there is an increase in estimated abundance in comparison with estimates from 2022 and a sharp decrease for block C. Block C also showed largest change in abundance in comparison to previous years. The estimates for this block in 2023 are associated with larger CVs compared to the estimates for the other two blocks in 2023 (Table 12, Figure 12).Figure 12 shows comparison between current estimates and estimates of the abundance from the previous report. The current results are comparable with the previous estimates. The comparison with the estimates from the report prior to 2023 is not possible, as all the abundance estimations prior to Paxton et al. 2023 included block G in the analysis.

Table 12,. Estimated number of individuals (N, in thousands) per block (block and year) with standard errors (SE) and lower (LCL) and upper (UCL) confidence levels. Coefficient of variation (CV) is also

provided for the results from this analysis. The orange values apply to estimates reported in Paxton et al. 2023. All estimates are based on sightings from all blocks: A, C, E.

Label	N	SE	CV	LCI	UCI	N	CV	LCI	UCI
	This report					Paxton et al. 2023			
A-2017	50.3	21.4	0.4	22.2	114.0	47.9	0.4	21.1	109.0
A-2018	82.2	24.8	0.3	45.7	147.7	78.2	0.3	43.1	141.8
A-2019	77.7	30.6	0.4	36.3	166.4	74.2	0.4	34.5	159.4
A-2021	44.5	25.0	0.6	15.6	126.8	44.3	0.5	15.6	126.1
A-2022	38.6	14.7	0.4	18.5	80.8	25.8	0.4	10.8	61.8
A-2023	58.6	27.4	0.5	23.7	144.6				
C-2017	44.9	18.4	0.4	20.2	99.9	44.1	19.8	97.9	19.9
C-2018	37.4	21.4	0.6	12.6	111.2	36.8	12.3	109.2	12.4
C-2019	26.0	15.1	0.6	8.6	78.5	25.5	8.4	77.1	8.4
C-2022	157.1	64.4	0.4	70.6	349.5	167.8	74.2	379.4	74.2
C-2023	33.0	22.1	0.7	9.5	114.8				
E-2017	44.2	22.8	0.5	16.6	117.9	42.2	15.7	112.7	15.8
E-2018	39.9	23.4	0.6	13.4	118.8	39.2	13.2	116.6	13.2
E-2019	31.1	15.6	0.5	12.1	79.9	31.2	12.1	80.2	12.2
E-2022	45.6	35.4	0.8	11.3	184.2	22.9	5.2	99.8	5.2
E-2023	148.7	60.7	0.4	66.7	331.5				

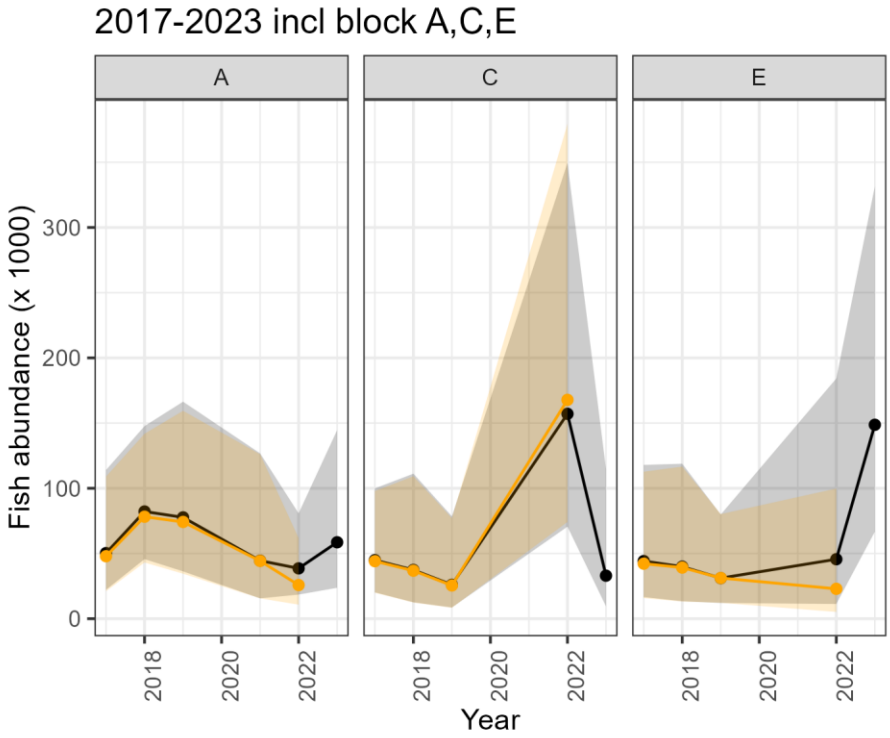

Figure 12. Estimated abundance of BFT for surveyed years and blocks. Black colours show estimates from this study: dots show mean values and ribbon show upper and lower confidence limits of the 95% confidence interval. Orange colour shows estimates from the previous report (Paxton et al. 2023).

4.1.2.3 Estimated biomass for years 2017-2023.

The biomass estimates are presented in Table 13 and Figure 13. The estimates for the previous years based on the newest detection function are comparable with the estimates from the previous reports. There is no increase in biomass in block A in 2023 despite the increase in abundance from 2022. There is a sharp decrease in biomass in block E and sharp increase in block C following these trends in abundance. The comparison with the estimates from the report prior to 2023 is not possible, as all the biomass estimations prior to Paxton et al. 2023 included block G in the analysis.

Table 13. Estimated biomass (B, in tonnes) per block (block and year) with standard errors (SE) and lower (LCL) and upper (UCL) confidence levels. Coefficient of variation (CV) is also provided for the results from this analysis. The orange values apply to estimates reported in Paxton et al. 2023. All estimates are based on sightings from all blocks: A, C, E.

Label	B	SE	CV	LCI	UCI	N	CV	LCI	UCI
	This report					Paxton et al. 2023			
A-2017	8665	3790	0.4	3747	20037	8927	0.43	3879	20546
A-2018	14499	4451	0.3	7974	26364	14857	0.3	8227	26828
A-2019	12858	5103	0.4	5973	27678	13268	0.39	6202	28387
A-2021	7287	4002	0.5	2605	20387	7667	0.53	2832	20760
A-2022	10554	4805	0.5	4408	25272	11903	0.43	5129	27627
A-2023	10877	5314	0.5	4256	27799				
C-2017	6970	2812	0.4	3158	15382	7691	0.38	3620	16338
C-2018	5221	3021	0.6	1735	15712	5822	0.55	2022	16764
C-2019	3175	1850	0.6	1044	9661	3549	0.56	1198	10513
C-2022	10735	4594	0.4	4663	24718	6878	0.41	3065	15436
C-2023	4036	2750	0.7	1136	14337				
E-2017	6348	3699	0.6	2131	18904	5639	0.58	1899	16750
E-2018	3852	2196	0.6	1331	11147	4423	0.54	1601	12215
E-2019	3383	1699	0.5	1313	8713	3063	0.46	1268	7396
E-2022	2115	1603	0.8	539	8301	1346	0.74	352	5149
E-2023	14897	6565	0.4	6277	35354				

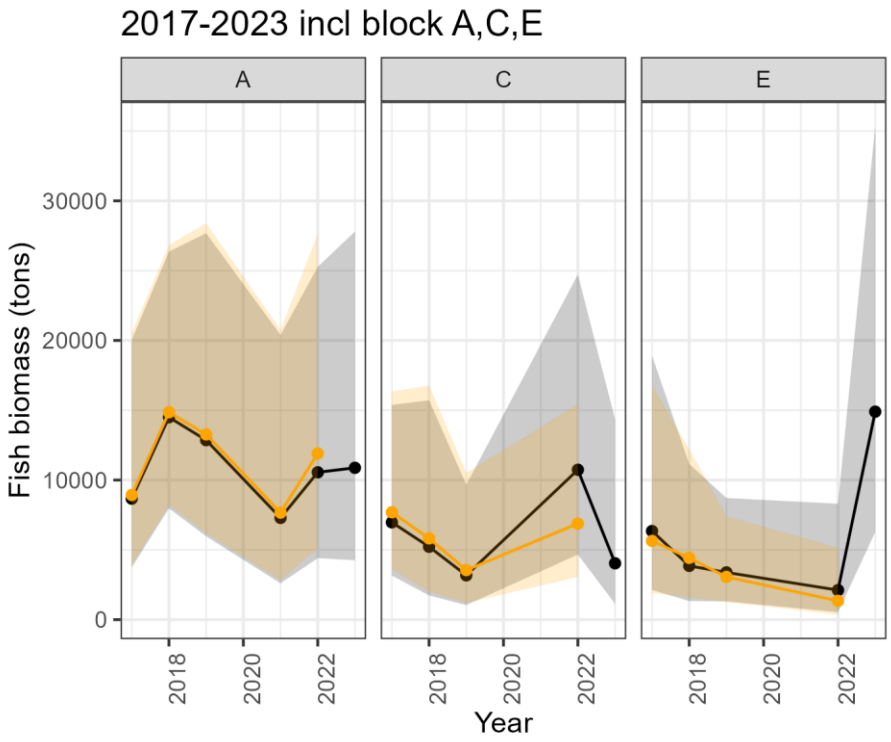

Figure 13. Estimated biomass (in tonnes) of BFT for surveyed years and blocks. Black colours show estimates from this study: dots show mean values and ribbon show upper and lower confidence limits of the 95% confidence interval. Orange colour shows estimates from the previous report (Paxton et al. 2023.

4.1.3 Comparison between Task 1A and Task 1B

The detection function based on all four blocks (A, C, E and G) is based on 167 sightings. Excluding area G leads to the reduction of the number of sightings to 155. Comparison of the average probability of detection and uncertainty around this parameter shows that excluding area G has little effect on the estimate of this parameter (Table 14). This is also reflected in comparable estimates of abundance and biomass based on these two different datasets (Figure 14, Figure 15).

Table 14. Comparison of the detection function parameters (probability of detection, p) between detection functions including and excluding area G, based on sightings from 2017-2023.

Detection function	Average p estimate	Average p SE	Average p CV
A,C,E,G - abundance	0.33	0.035	0.11
A,C,E - abundance	0.32	0.033	0.10
A,C,E,G - biomass	0.48	0.028	0.06
A,C,E - biomass	0.47	0.028	0.06

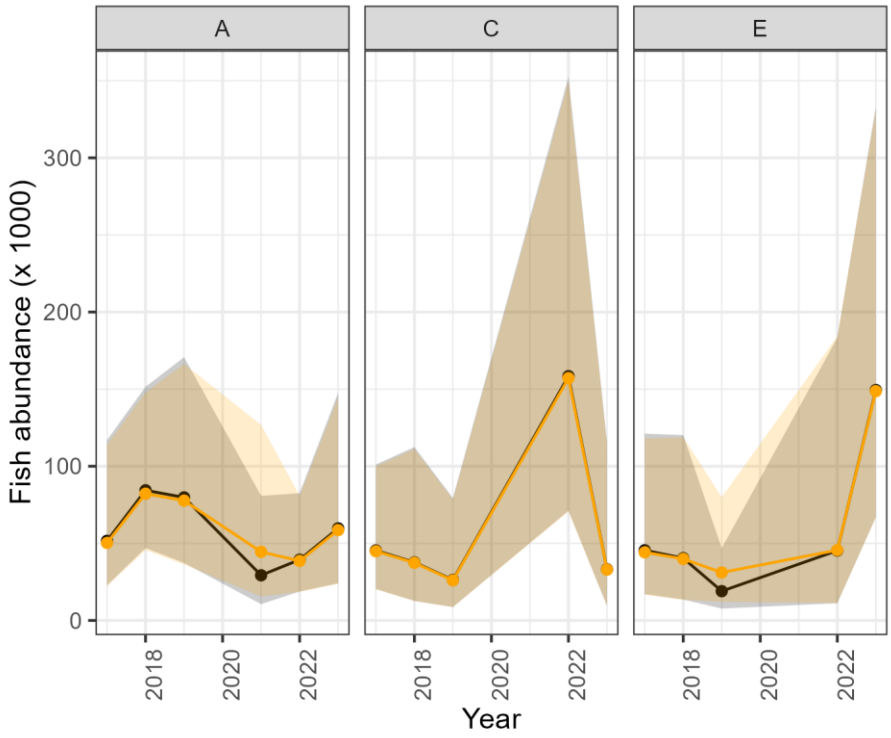

Figure 14. Estimated abundance of BFT for surveyed years and blocks. Black colours show estimates based on all four blocks (A, C, E and G): dots show mean values and ribbon show upper and lower confidence limits of the 95% confidence interval. Orange colour shows estimates based on three blocks (A, C, E).

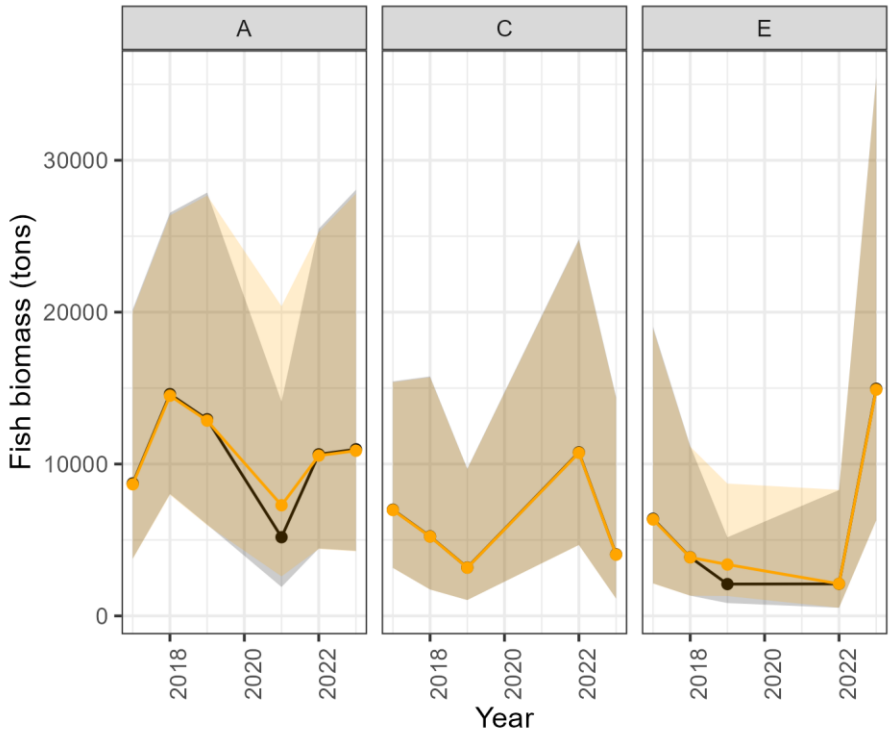

Figure 15. Estimated biomass (in tons) of BFT for surveyed years and blocks. Black colours show estimates based on all four blocks (A, C, E and G): dots show mean values and ribbon show upper and lower confidence limits of the 95% confidence interval. Orange colour shows estimates based on three blocks (A, C, E).

4.1.4 Task 2

The results assuming an identical function to last year are given in Table 15, Figure 16 (abundance) and Table 16, Figure 17 (biomass) respectively. For blocks C and E the point estimates are very similar to those from Task 1A (Table 8) for 2023. The block A estimates are different although there is substantial overlap in confidence intervals of the two estimates.

Table 15. Estimated number of individuals (in thousands) per block (block and year) with standard errors (SE) and lower (LCL) and upper (UCL) confidence levels based on the parameter estimates from analysis up to the 2022 data inclusive. Coefficient of variation (CV) is also provided for the results from this analysis. All estimates are based on sightings from all blocks: A, C, E and G from previous years.

Label	N	SE	CV	LCI	UCI
A-2023	39.1	23.3	0.6	13.0	117.3
C-2023	35.1	23.8	0.7	10.0	123.7
E-2023	158.3	67.3	0.4	69.2	362.1

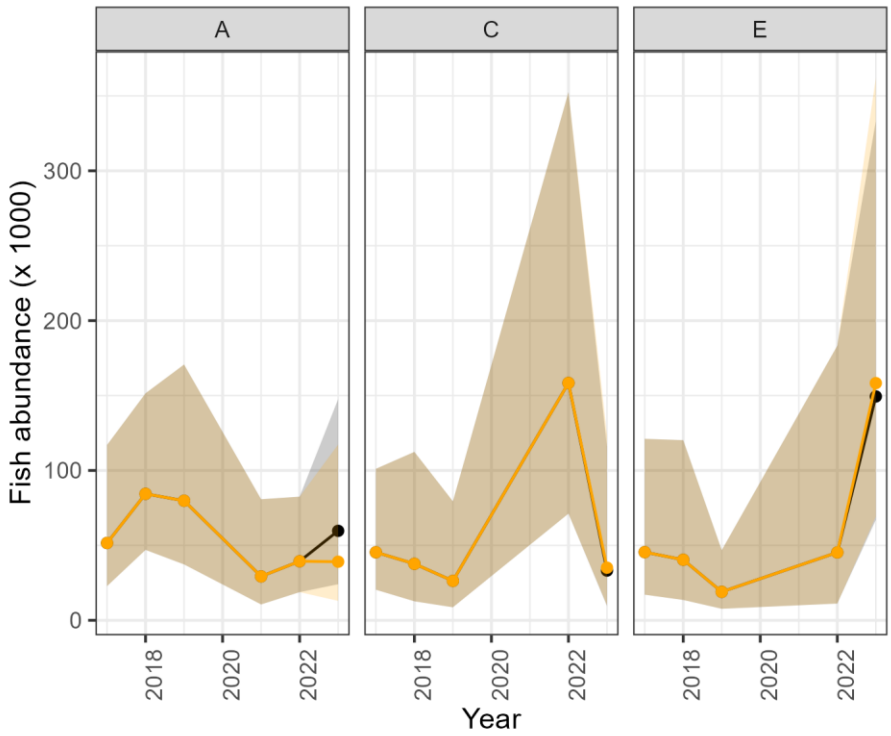

Figure 16. Estimated abundance (in thousands) of BFT for surveyed years and blocks. Black colours show estimates based on all four blocks (A, C, E and G) for Task 1A: dots show mean values and ribbon show

upper and lower confidence limits of the 95% confidence interval. Orange colour shows estimates based in Task 2.

The biomass results are very similar to the pattern in the abundance estimates for all three blocks and to estimates from Task 1A (Table 9). The largest discrepancies in the estimates between Task 1A and 2 are for blocks A and E but both well within the confidence intervals.

Table 16. Estimated biomass (B, in tonnes) per block (block and year) with standard errors (SE) and lower (LCL) and upper (UCL) confidence levels based on the parameter estimates from analysis up to the 2022 data inclusive. Coefficient of variation (CV) is also provided for the results from this analysis. All estimates are based on sightings from all blocks: A, C, E and G.

Label	N	SE	CV	LCI	UCI
A-2023	7513.3	5624.2	0.75	2007.3	28122.5
C-2023	3793.5	2601	0.69	1063.5	13531.4
E-2023	14026.2	6352	0.45	5810	33861.1

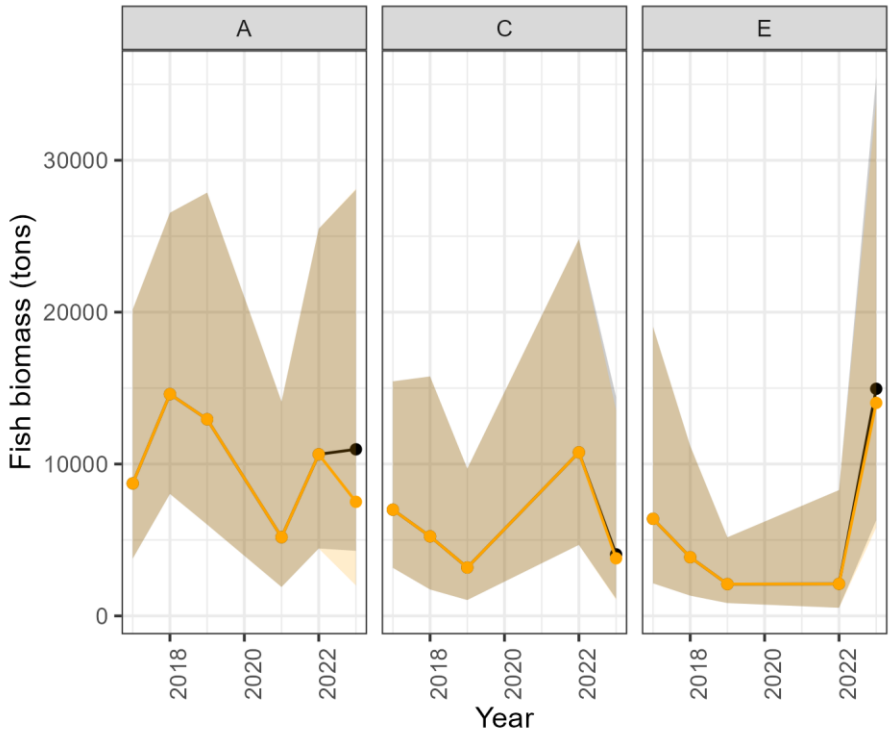

Figure 17. Estimated biomass (in tonnes) of BFT for surveyed years and blocks. Black colours show estimates based on all four blocks (A, C, E and G) for Task 1A: dots show mean values and ribbon show upper and lower confidence limits of the 95% confidence interval. Orange colour shows estimates based in Task 2.

5 Discussion

It should be stressed that the estimates given here are based on sightings of fish observed at the surface or close enough to the surface to be detected (relative abundance and biomass) and so may be very different to the actual number/biomass of fish.

The analysis presented in Task 1 revealed that there is little difference between the abundance and biomass estimates between analysis based on all four blocks (A, C, E and G) and just three blocks (A, C, E) and both estimates are well within the confidence intervals of each other. One would expect the uncertainties around the estimate probability of detection to decrease the larger the number of detections. There was, however, no change in the estimated uncertainties. Keeping the detection function based on all four blocks is, however, consistent with the biomass and abundance estimates of the ICCAT GBYP programme and useful in case block G is surveyed again in the future.

Task 1 calculated four detection functions: based on the size of the detected schools including and excluding sightings from area G; and based on biomass of the detected schools including and excluding sightings from area G. The best detection functions for all four blocks included log of the size/biomass of the detected schools and company conducting the survey. This is consistent with the detection functions reported in the previous years (Chudzinska et al. 2021, Chudzinska et al. 2022, Paxton et al. 2023). The detection functions which included block – year combinations and log of the size/biomass were having comparable AICs but note that company and block-year are correlated as most blocks are surveyed by specific companies only. The detailed explanation why company was the best predictor is given in Paxton et al. (2023) and is related to varying distributions of the observed distances between companies.

The actualisation of the tuna indices for 2023 showed an increase in BFT abundance in blocks A and E and decrease in block C. The estimates for block E are associated with large confidence intervals most likely since only part of the block was surveyed. This resulted in lower number of sightings in this block in comparison to previous years. The expected school size in this block is also much higher in 2023 than in 2022, hence increase in abundance and larger uncertainties. The encounter rate in block A was higher in 2023 than 2022 but lower in 2023 than 2022 in the two other blocks, which is reflected in the above-mentioned trend in abundance.

The probability of detection in block A in 2023 was much lower than in the previous surveyed year 2022 (0.32 and 0.60 respectively) but comparable in the remaining two blocks (0.35 and 0.40 in block C and 0.38 and 0.28 in block E respectively) between the last two years (2022 and 2023).

While adding new data (here, new surveyed year) and calculating a new detection function based on updated data, standard error and confidence intervals for the previous years can be updated and, frequently, reduced. The approach used in Task 2 does not allow for such updates as the calculation is based on detection function on a reduced data set (i.e. not including sightings from 2023). We, therefore, recommend continuing using the approach from Task 1A instead of Task 2, especially that the best detection function contains the same covariates (here company) each year of the analysis.

CREEM has been analysing the BFT sightings since many years and received the data from various companies across the years. Although the consistency of data delivery and reporting has improved significantly over the years, a few issues still occur. The effort in block A does not always include all data on start and end of each transect and clear indication when planes left and when rejoined the transect. Such a check of the data before delivery would greatly improve the data analysis. The unit of reported biomass is not always consistent between sightings, biomass is reported both in tonnes and in kg for the same survey. Finally, data formatting may differ within the same survey: decimal places are frequently separated both by comma and dot in the same document. A standardized way of data entry would also greatly improve data analysis and reduce potential errors.

6 Conclusions and recommendations

- The actualisation of the tuna indices for 2023 showed an increase in BFT abundance in blocks A and E and decrease in block C.
- Surveying only part of block E resulted in large uncertainties in abundance and biomass estimates for that region.
- We recommend basing all future estimates of biomass and abundance on all sightings between 2017-2023, including block G.
- We recommend basing all future estimates of biomass and abundance on a new detection function updated if new data appear.

7 Acknowledgements

This work has been carried out under the ICCAT Atlantic-Wide Research Programme for BFT (GBYP), which is funded by the European Union, several ICCAT CPCs, the ICCAT Secretariat, and other entities (see https://www.iccat.int/gbyp/en/overview.asp). The content of this paper does not necessarily reflect ICCAT's point of view or that of any of the other sponsors, who carry no responsibility. In addition, it does not indicate the Commission's future policy in this area.

8 References

AirPerigord. 2023. Final Report - Deliverable #5. The Atlantic-wide research programme for bluefin tuna GBYP- Phase 12 - Zone A - Mer des Baléares. Short term contract for biological studies (ICCAT GBYP 06/2023).

Akaike, H. 1987. Factor analysis and AIC. Pages 317-332 Psychometrika.

Buckland, S. T., D. R. Anderson, K. P. Burnham, J. L. Laake, D. L. Borchers, and L. Thomas. 2001. Introduction to Distance Sampling. Estimating abundance of biological populations. Oxford University Press, Oxford.

Chudzinska, M., L. Burt, D. Borchers, D. Miller, and S. Buckland. 2021. Design-based inference to estimate density, abundance and biomass of bluefin tuna. Reanalysis of 2010-2019

Aerial Surveys. Report number CREEM-2021-03. Provided to ICCAT, September 2021 (Unpublished).

Chudzinska, M., L. Burt, and S. Buckland. 2022. Design-based inference to estimate density, abundance and biomass of bluefin tuna. Reanalysis of 2017-2021 Aerial urveys of Region A. Report number CREEM-2022-03. Provided to ICCAT, July 2022 (Unpublished).

Laake, J., D. Borchers, L. Thomas, D. Miller, and J. Bishop. 2022. mrds: mark–recapture distance sampling. R package version 2.2.8. https://cran.r-project.org/package=mrds.

Marques, T. A., L. Thomas, S. G. Fancy, and S. T. Buckland. 2007. Improving estimates of bird density using multiple-covariate distance sampling. The Auk **124**:1229-1243.

Miller, D. L. 2022. Package 'Distance'. Versión 0.9 **6**.

Miller, D. L., E. Rexstad, L. Thomas, L. Marshall, and J. L. Laake. 2019. Distance Sampling in R. Journal of Statistical Software **89**:1 - 28.

Paxton, C. G. M., C. S. Oedekoven, M. Chudzinska, M. Pilar Tugores Ferrá, and D. Alvarez-Berastegui. 2023. Design- and model-based inference to estimate density, abundance and distribution of BFT in the Mediterranean Sea. Report number CREEM-2023-04. Provided to ICCAT, July 2023 (Unpublished).

R Core Team. 2023. R: A Language and Environment for Statisical Computing. R Foundation for Statistical Computing.

Unimar, and AerialBanners. 2023a. Aerial survey for the monitoring of bluefin tuna spawning aggregations in the Mediterranean Sea (ICCAT GBYP - Phase 13) - ICCAT GBYP circular # G-0428/2023 - Area C.

Unimar, and AerialBanners. 2023b. Aerial survey for the monitoring of bluefin tuna spawning aggregations in the Mediterranean Sea (ICCAT GBYP - Phase 13) - ICCAT GBYP circular # G-0428/2023 - Area E.